Constant Strain Rate and Peri-Implant Bone Modeling: An In Vivo Longitudinal Micro-CT Analysis

Els De Smet, DDS, PhD;* Siegfried V. N. Jaecques, PhD;† Martine Wevers, PhD;‡ Jos Vander Sloten, PhD;§ Ignace E. Naert, DDS, PhD¶

ABSTRACT

Background: Strain, frequency, loading time, and strain rate, among others, determine mechanical parameters in osteogenic loading. We showed a significant osteogenic effect on bone mass (BM) by daily peri-implant loading at 1.600 με.s^{-1} after 4 weeks.

Purpose: To study the peri-implant osteogenic effect of frequency and strain in the guinea pig tibia by in vivo longitudinal micro-computed tomography (CT) analysis.

Material and Methods: One week after implant installation in both hind limb tibiae, one implant was loaded daily for 10′ during 4 weeks, while the other served as control. Frequencies (3, 10, and 30 Hz) and strains varied alike in the three series to keep the strain rate constant at 1.600 με.s^{-1}. In vivo micro-CT scans were taken of both tibiae: 1 week after implantation but before loading (v1) and after 2 (v2) and 4 weeks (v3) of loading as well as postmortem (pm). BM (BM (%) bone-occupied area fraction) was calculated as well as the difference between test and control sides (delta BM)

Results: All implants ($n = 78$) were clinically stable at 4 weeks. Significant increase in BM was measured between v1 and v2 ($p < .0001$) and between v1 and v3 ($p < .0001$). A significant positive effect of loading on delta BM was observed in the distal peri-implant marrow 500 Region of Interest already 2 weeks after loading ($p = .01$) and was significantly larger (11%) in series 1 compared with series 2 ($p = .006$) and 3 ($p = .016$).

Conclusions: Within the constraints of constant loading time and strain rate, the effect of early implant loading on the peri-implant bone is strongly dependent on strain and frequency. This cortical bone model has shown to be most sensitive for high force loading at low frequency.

KEY WORDS: animal study, early loading, frequency, guinea pig, implant, in vivo micro-CT

INTRODUCTION

Important parameters for osteogenic (bone forming) mechanical loading can be identified from the literature (e.g., strain rate, peak strain, and number of cycles/duration).[1] The effect of low-amplitude and high-frequency mechanical signals on cortical and cancellous bone was investigated by Rubin and colleagues[2] in sheep tibia. They promoted these loading parameters as highly osteogenic. Besides, these were minimally traumatic for mineral tissues and experimental animals. They found that when a load of only a few grams was administered at high frequencies for a few minutes a day, the bone mass (BM) significantly increased. They concluded that strain rate – as a product of strain (proportional to the amplitude of the force applied onto the bone) and

*Dentist, Dr. Dental Science, Department of Prosthetic Dentistry/BIOMAT Research Cluster, School of Dentistry, Oral Pathology and Maxillofacial Surgery, Faculty of Medicine, K.U. Leuven, Leuven, Belgium; †Mech. Eng., Division of Biomechanics and Engineering Design, Department of Mechanical Engineering, K.U. Leuven, Leuven, Belgium; ‡Mech. Eng., Department of Metallurgy and Materials Engineering, K.U. Leuven, Leuven, Belgium; §Mech. Eng., Division of Biomechanics and Engineering Design, Department of Mechanical Engineering, K.U. Leuven, Leuven, Belgium; ¶Dentist, Dr. Dental Science, Head, Department of Prosthetic Dentistry/BIOMAT Research Cluster, School of Dentistry, Oral Pathology and Maxillofacial Surgery, Faculty of Medicine, K.U. Leuven, Leuven, Belgium

Reprint requests: Dr. Ignace Naert, Department of Prosthetic Dentistry/BIOMAT Research Cluster, School of Dentistry, Oral Pathology and Maxillofacial Surgery, Faculty of Medicine, K.U. Leuven, Kapucijnenvoer, 7 box 7001, 3000 Leuven, Belgium; e-mail: ignace.naert@med.kuleuven.ac.be

DOI 10.1111/j.1708-8208.2011.00375.x

frequency of the applied load – is the determining mechanical parameter in osteogenic loading.

In implant dentistry, early and immediate implant loading became popular since the last decade. The local mechanical loading situation is supposed to strongly determine the processes of tissue differentiation and the coupled process of bone formation and resorption around implants.[3–5] Preliminary results did show a positive effect on BM for loaded implants in the medullar cavity.[6] We found in a guinea pig experiment on early loading of endosseous implants that a strain rate of 1.600 $\mu\varepsilon.s^{-1}$ evoked the most osteogenic effect on peri-implant BM 4 weeks after daily loading.[7]

The hypothesis formulated for this study is that a high strain at low-frequency loading should have an equal osteogenic effect as a low strain at high frequency. Three series of guinea pigs subjected to early loading with the same strain rate (1.600 $\mu\varepsilon.s^{-1}$) and equal loading time (10′) but with varying frequencies (3–10–30 Hz) – and inversely proportional force amplitudes resulting in strains – were performed. Microfocus computed tomography (CT) was used to monitor the in vivo longitudinal follow-up of the osteogenic effect around the implants.

MATERIALS AND METHODS

Implants

Customized AstraTech implants (AstraTech Dental, Mölndal, Sweden) of Ti6Al4V were used (Figure 1). The endosseous part was screw-shaped with an outer diameter of 1.8 mm and length of 5 mm to allow bicortical fixation for good primary stability. The surface was TiO_2-blasted resulting a surface roughness (Ra = 1.74 μm). The implants were hollowed to a maximum extent without jeopardizing the implant's strength in order to reduce streak artifacts on micro-CT images caused by the titanium. The conical and percutaneous parts were as-machined and allowed a connection for additional devices by friction and screw tightening.

Surgical Procedure

Three series of skeletally mature male guinea pigs (average $n = 11$) were selected to receive the percutaneous customized implants in the distal part of both hind limb tibiae. Surgery was performed under general anesthesia (Ketamine Ceva 1000® [Ceva Animal Care, Brussels, Belgium] 50 mg/kg I.M. and Xyl-M® [V.D.K., Arendonk, Belgium] 2% solution, 0.25 mL/kg I.M.). A longitudinal incision was made on the medial side of the tibia just above the ankle joint. Both cortices of the tibia were perforated with low rotational speed under profound external saline cooling to a diameter slightly smaller (0.3 mm) than the implant's diameter to obtain a good primary stability. Implants were inserted by manual torque. Resorbable sutures (Vicryl® 3–0, Ethicon GmbH, Norderstadt, Germany) were used to close the incisions. Postoperatively, the guinea pigs received doxycycline (Vibravet®, Pfizer, Brussels, Belgium) (0.5 mg/kg p.o.) during 5 days for infection prevention. Additionally, strict cage hygiene was maintained by daily changing the bedding material during the study period. Buprenorfin (Temgesic®, Reckit & Coleman, Hull, UK) (0.05 mg/kg S.C.) was used for analgesia.

Figure 1 Customized Ti6Al4V implant (AstraTech Dental, Mölndal, Sweden), TiO_2-blasted resulting in a moderate roughened topography (Ra = 1.74 μm). Conical and as-machined permucosal neck to allow stable loading device connection.

Mechanical Loading

Mechanical loading started 1 week after implant installation to allow skin healing before manipulation with the loading device. In each animal, one implant was loaded while the contralateral implant served as unloaded control. Implant loading was ad random allocated to the right or left tibia and served as test implant. Loading was performed through a sinusoidally varying bending moment applied with a force-controlled

TABLE 1 Mechanical Parameters of the Early Loading Experiment of Screw-Shaped Ti Implants in the Distal Tibia of Guinea Pigs

Series	Cycle Number (*n*)	Force (N)	Strain (με)	Frequency (Hz)	Strain Rate ($\mu\varepsilon.s^{-1}$)
1	1.800	2	533	3	1.600
2	6.000	0.6	160	10	1.600
3	18.000	0.2	53	30	1.600

electromechanical shaker (Model 4810, Brüel and Kjaer, Naerum, Denmark). All the three series received a load regimen of 10 min/day, 5 days/week, during 4 successive weeks.

The strains, as a result of the forces, listed in Table 1 were calculated from cadaver load-strain calibration experiments, repeated three times.[7] In brief, the strain gauge (FLG-02–11 of TML, Tokyo Sokki Kenkyujo Co. Ltd, Tokyo, Japan) was bonded on the medial bone surface of the tibia, in the loading direction as close as 1.3 mm from the implant's body. No closer contact to the implant's body was possible because of the dimensions of the strain gauge grid. The same stimulator device that functioned for the final experiments was used. The measured strains increased linearly with the forces applied. From simplified finite element calculations, strains in the cortical bone in the immediate vicinity of the implant were estimated to be in the order of 2,000–3,000 με for a force of 6 N. This is 1.3 to two times the strains quantified at a 1.3-mm distance from the implant.[7]

Varying strains, as the result of implant loading, were combined with varying loading frequencies to result in a constant strain rate of 1,600 $\mu\varepsilon.s^{-1}$ in each of the three series. The number of cycles was adjusted correspondingly for all the three series to fit the 10′ loading time. During loading, the animals were under full inhalation anesthesia (Fluothane®, halothane, Zeneca, Belgium/Forene®, isoflurane, Abbott, Queensborough, Kent, UK), and the hind limb was firmly fixed by an alginate casting to the base plate of the stimulator to ensure reproducible mechanical loading. The horizontal lever arm was attached onto the implant, in alignment with the long axis of the tibia. At a distance of 20 mm, distally from the implant, the electromechanical shaker applied a sinusoidally varying force through a piezo load cell model PCB 208B03 (PCB Piezotronics, Depew, NY, USA). Force was transferred from the load cell to the lever through an aluminum-threaded pin. A preload of approximately 1 N ensured calibration through continuous contact with the lever. Signals from the load cell were amplified by a PCB 480D06 amplifier (10-second time constant) (PCB Piezotronics) and captured by a Keithley 1702AO 12 A/D data acquisition card (Keithley Instruments B.V., Sint-Pieters-Leeuw, Belgium). The same card was also used to send the control signal for the shaker through a direct current coupled power amplifier (custom-made). Control software, including a force-controlled feedback loop, data acquisition, and data visualization, was implemented as a TestPoint application on a Pentium-100 PC running under MS Windows95. Normal cage activity was allowed between loading sessions.

Micro-CT

The micro-CT device used was a HOMX 161 microfocus x-ray source (Philips x-ray, Hamburg, Germany) equipped with an AEA Tomohawk rotating sample stage and image acquisition and slice reconstruction software. In vivo micro-CT scans, both test and control sides were taken postoperatively before loading was started (baseline) (v1), 2 weeks after loading (v2), and at the end of the study, 4 weeks after loading (v3). For the in vivo micro-CT scans, a smoothing kernel (1,2,1) was used during slice reconstruction to reduce the noise. At the detector, a combination of a 2 mm-thick aluminum and a 10 mm-thick polymethylmethacrylate filter was used to reduce the streak artifacts caused by the titanium implants. Guinea pigs were brought under general injection anesthesia (Ketamine Ceva 1000, 50 mg/kg I.M., and Xyl-M 2% solution, 0.25 mL/kg I.M.) A custom-made sample holder kept the guinea pig laterally reclined with the head down and the hind leg extended upward, keeping the tibia horizontal and the implant vertical. The sample holder contained a coping to hold the implant vertically in the center of rotation. The tibia rotated around the implant. Limited radiation exposure was considered. The guinea pig's body, head, and

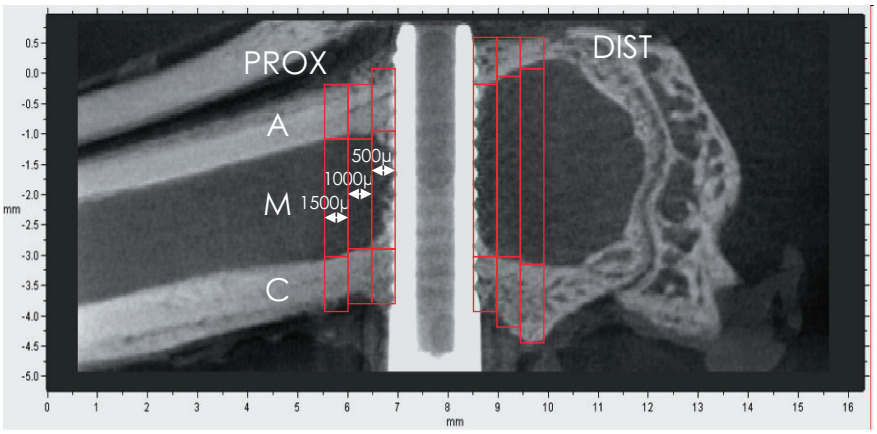

Figure 2 Example of an in vivo micro-computed tomography (CT) slice of a guinea pig tibia with percutaneous implant with indicated Regions of Interest (ROIs) for bone mass measurements. Quantification of bone mass (%) was performed on these longitudinal images of the proximal and distal halves of the micro-CT slices, at 3 × 3 ROIs of interest (ROI): 500, 1,000, and 1,500 μm away from the proximal and distal implant surfaces for the cervical cortex (C500, C1000, and C1500), medullar cavity (M500, M1000, and M1500), and the apical cortex (A500, A1000, and A1500).

contralateral hind limb were covered with a lead shield to provide radiation protection. The animals were sacrificed by asphyxiation with CO_2, the tibiae were dissected, and postmortem (pm) micro-CT scans, using different scan parameters resulting in a higher resolution, were taken of the dissected tibiae-with-implant specimens. The micro-CT protocol is in detail described in Jaecques and colleagues.[8] Micro-CT slices were reconstructed in the loading direction parallel to the longitudinal direction of the tibiae and to the long axis of the implants. A micro-CT slice through the middle of the implant was selected for each time point (v1, v2, v3, pm).

ANALYSES

Micro-CT Morphometrical Analysis

The micro-CT slice images were imported in an image analysis system (Q-win®, Leica BV, Rijswijk, The Netherlands). To segment the images for bone, a threshold defining bone was set manually and kept constant for all the images created with the same scan parameters. On these colored binary images, BM was calculated as the bone-occupied area fraction per standardized ROI of interest (ROI). BM (%) = (area of bone in the ROI (μm^2)/ROI area [μm^2]) × 100. The effect of loading on new bone formation was quantified by subtracting BM around control from those of test implants and were expressed as delta BM (delta BM = BM at the loaded minus BM at the control side). ROIs were defined in the cervical peri-implant cortex (C), marrow cavity (M), and apical cortex (A) at 500, 1,000, and 1,500 μm from the implant body at the distal and proximal sides of the implant (Figure 2). Those ROIs are referred to as, for example, M500, M1000, and M1500 for the marrow cavity.

Statistical Analysis

In order to obtain valid inferences about the mean evolution of BM and its relationship with the variables of interest, the correlation between measurements on the same guinea pig (control/test and across time) should be accounted for. A multivariate linear model in SAS® 9.1 (SAS Institute Inc., Cary, NC, USA) was fitted to study the joint evolution of BM in the loaded and nonloaded tibiae over time. The period of 2 weeks between the micro-CT sessions was used as time variable. The model included loading, period, and their two-way interaction as fixed effects. In order to study the effect of the different loading parameters per series on the evolution of BM, a multivariate model was also fitted. The pm micro-CT data were analyzed by fitting a linear regression model with a random effect to account for the correlation between measurements on the same guinea pig (test/control). For both the latter, the model included series, loading, and their interaction terms as fixed effects. To adjust for multiple testing, the Tukey procedure was used. The level of significance was set at $\alpha = 5\%$.

RESULTS

Animal and Implant Outcome

All animals survived well during the course of the experiment. Due to the 1-week healing period of the skin, preceding the implant loading regimen, the skin remained healthy over the whole course of the experiment (5 weeks). Test and control implants ($n = 78$) integrated uneventfully. At sacrifice, no clinical mobility of any of the implants could be observed.

Typical results of two-dimensional-reconstructed CT slices clearly show progressive bone modeling over 4 weeks at the test side (Figure 3). On the in vivo images, somewhat streak artifacts and general noise could be seen. However, the geometry of the cortical bone on the in vivo image matched the pm image quite well. The micro-CT images were also serviceable as input to generate individualized finite element models, which will be reported elsewhere. It was found that for the medullar cavity, new bone was formed along the implant surface, originating from the endosteum of the upper and lower cortex of the tibia mimicking the principle of osteoconduction. Not only along the implant surface but also along the endosteum – proximal and distal from the implant – new bone had formed in the medullar cavity.

Morphometrical differences between test and control peri-implant BM were mainly observed at the distal side of the implant in the medullar cavity, which is in the same direction of the lever arm that was positioned and where mechanical loading was applied. Data for the cervical and apical ROI did only occasionally lead to significant differences for test and control implants and will not further be addressed here.

In Vivo Bone Mass Evolution

BM (%) evolution over time, averaged over all the three series at the medullar ROI (MROI), is shown for test and distal sides in Figure 4. A significant increase in BM at the M500 ROI was observed after 2 ($p < .0001$) and 4 weeks ($p < .0001$), but not between 2 and 4 weeks of loading. There was a significant difference in BM between series 1 and 3 in favor of the former ($p = .03$). For the M1000 ROI, there was also a significant increase of BM after 2 ($p = .0005$) and 4 weeks, respectively

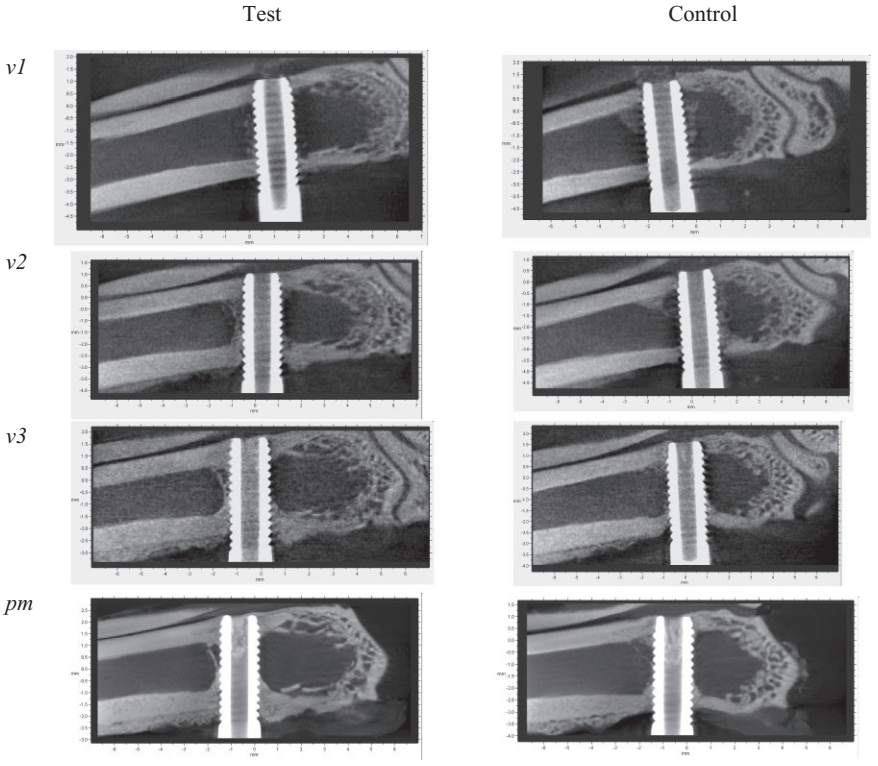

Figure 3 Example of two-dimensional (2D) reconstructed in vivo computed tomography (CT) slices of test and control tibiae of the same guinea pig postoperatively; before (*v1*), after 2 weeks (*v2*), and after 4 weeks of loading (*v3*). 2D-reconstructed postmortem CT slices (*pm*) were prepared after sacrificing the guinea pigs and dissecting the bone with implant specimens.

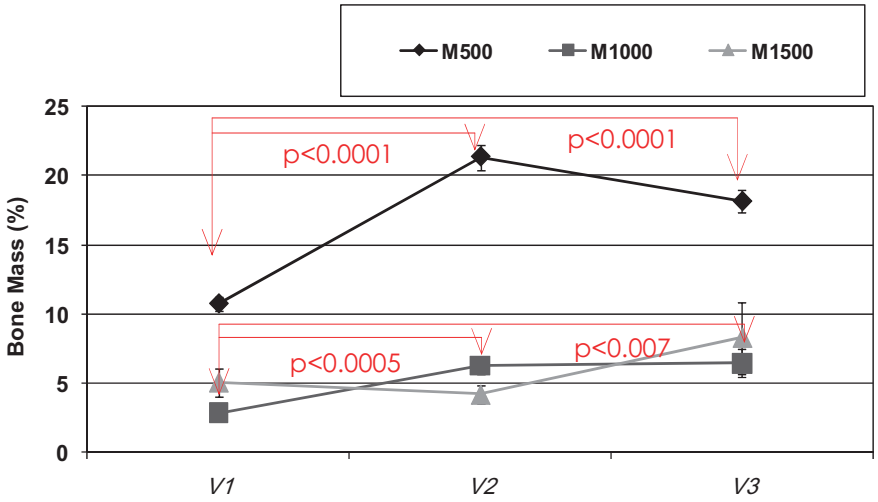

Figure 4 Bone mass (%) averaged over all the three series (test only) is shown in function of time for the medullar Region of Interest (ROI) at the distal sides (most pronounced effect). For the M500 ROI, which is the one closest to the implant in the bone marrow cavity, a clear increase in bone mass can be shown from time point *v1* until *v2* ($p < .0001$) and *v3* ($p < .0001$). For the ROI M1000, also an increase in mean bone mass could be shown from *v1* until *v2* ($p < .0005$) and *v3* ($p < .007$). For the ROI M1500, also an increase in mean bone mass could be shown but did not reach any significance.

($p = .007$). Further away from the implant at the M1500 ROI, significant differences neither in BM nor between the three series were found.

Delta Bone Mass

At the M500 ROI, a significant effect of loading (delta BM) could be found already after 2 weeks (v2) ($p = .01$) as well as in the more detailed pm images ($p = .01$). At the M1000 and 1500 ROI, no significant loading effect could be observed in the in vivo micro-CT images.

Delta BM in the M500 ROI, averaged over proximal and distal sides in the more detailed pm micro-CT images, was significantly larger (11%) in series 1 than in series 2 ($p = .006$) and 3 ($p = .016$) (Table 2). At the M1000 and M1500 ROI, this difference was not present anymore, except for a marginal effect in series 2 and 3 in favor of the former ($p = .048$) at the M1500 ROI. In this model, keeping the strain rate and the loading duration constant, the effect of early mechanical loading increased with increasing force amplitude and decreasing frequency.

TABLE 2 Delta Bone Mass (SD), Averaged over Proximal and Distal Sides, Expressed as the Difference between Bone Mass for Test and Control Side ROI, Measured on Postmortem Micro-CT Slices

ROI	M500	M1000	M1500
Series 1	11.32% (3.3)*†	4.30% (2.1)	4.81% (2.3)
Series 2	0.76% (1.9)*	–1.31% (1.5)	0.97% (1.3)‡
Series 3	0.95% (2.3)†	–0.33% (2.0)	–0.37% (1.2)‡

Positive values mean gain in bone mass in favor of test sides, negative in favor of control sides. Values with the same sign ($^{\star},^{\dagger},^{\ddagger}$) are significantly different from each other ($p < .05$). ROI = Region of Interest.

DISCUSSION

The added value of the in vivo micro-CT methodology over histology is being able to perform a longitudinal follow-up of bone changes within the same small animals. This was the reason why a former contribution dealing with the histology on the same data set was supplemented with these micro-CT analyses.[9] The limiting factor in the former study was that only one time point could be investigated (at 4 weeks); thus, no analysis over time, within the same animal, was possible. The bone area fraction obtained through histology at 4 weeks corroborated well with those obtained through micro-CT analysis (pm). It is obvious that bone-to-implant contact analysis can only be performed well through histology because of the beam hardening effect of metal within the micro-CT images.

To explain bone adaptation to mechanical loading, Frost's[10] mechanostat focused on bone strain. He described a window of mechanical usage, which is defined by an upper boundary (1.500 με), called the minimum effective strain above which bone undergoes modeling and changes its structure in order to reduce

the local stress and strain. It has been shown that above a certain strain threshold, bone formation is initiated in cortical bone[11,12], and that with increasing strain, bone responds with new formation.[13,14] Excessive loads have been studied and even the borderline of the bone-implant failure value has been quantified in the rabbit model.[2] The strains, estimated from CT-based finite element models, associated with overload-induced resorption, were in the order of 4,200 με. Frost[15] considered 4,000 με a possible threshold for pathological overload, suggesting that higher strains would lead to the accumulation of bone microdamage (microcracks) in case of cyclic loading. In the guinea pig experiments, an increase in delta BM could be shown with increasing force amplitude.[6] From a generic finite element analysis of this guinea pig implant model, it was estimated that a force amplitude of 6 N caused peri-implant bone strains in the order of magnitude of 2,000–3,000 με next to the implant's body, which should be considered an osteogenic stimulus according to Frost's[10] mechanostat. From this simplified finite element model, it was obvious that the highest strains are observed next to the implant surface at the cortex (ROI 500 μm). Further away from the implant, the strains decreased resulting in less pronounced delta BM. The authors are aware of the fact that strains, as measured by strain gauges, can significantly underestimate the actual strains as measured using, for example, digital imaging techniques.[16]

With the HOMX 161 microfocus x-ray source and the AEA Tomohawk micro-CT system, microfocus CT scans of guinea pig tibiae with Ti6Al4V implants can be obtained in vivo with a quality approaching that obtained on micro-CT scans of dissected tibiae. However, care must be taken to reduce the radiation exposure to the maximum extent possible. No deterministic radiation side effects were clinically observed up to the end of the study. This is consistent with the reported absence of radiation effects when in vivo synchrotron x-ray microscopy is applied to the tibiae of rats.[17] Only limited literature data are available for guinea pigs. The radiation doses of 1.7 Gy administered in this study were well below the limit of 3 Gy per scan that was previously reported by our series as safe for short-term in vivo work on guinea pig tibiae with titanium implants.[18] Brouwers and colleagues.[19] found no radiation effect on structural parameters and bone marrow cells in the proximal tibia of rats after eight weekly scans.

Together with finite element modeling and computer simulations of the remodeling process,[8,20,21] in vivo micro-CT might contribute to the discussion on whether and how bone acts on the applied mechanical loading.

Noise was the limiting factor in the segmentation of the micro-CT slices. Along the whole implant surface, a thin artifact-affected layer was present, which influenced decision making in setting threshold for defining bone on the micro-CT slices. In vivo micro-CT slices showed more noise than pm images, resulting in a more troublesome segmentation. Metal artifacts are due to a combination of beam hardening, scatter, nonlinear partial volume effect, and noise.[22]

An aluminum filter was placed between the detector and specimen to reduce artifacts from the titanium. The filter reduced secondary radiation and suppressed to a major extent, but not completely, the streak artifacts. As a consequence, bone-to-implant contact could not be measured around the full metallic implants as shown earlier.[23]

It has been shown that bone responds especially to dynamic rather than to static loading.[4,24] This means that (cortical) bone (re)modeling is not solely dependent on strain but that cyclic loads have the potential to induce bone formation.[25] Mechanical loading parameters, such as strain rate,[26] frequency, number of loading cycles,[13,27] strain distribution, and gradient,[28] will all influence the bone's adaptive response. Strain rate can further be decomposed into strain and frequency. A positive relationship between loading frequency and bone formation has been demonstrated in several studies.[29,30]

In this study, in which a constant strain rate was applied, the effect of early mechanical loading increased with increasing force amplitude and decreasing frequency. For the high-frequency (30 Hz) loading (series 3), delta BM was small, whereas a significant larger delta BM for the low (3 Hz) frequency loading (series 1) was found. These results corroborate with the partially analyzed and reported data in De Smet and colleagues.[6]

Our hypothesis that a high strain at low-frequency loading did have an equal osteogenic effect as its inversed loading regimen had to be refuted.

In the ulna axial compression model in mice, a dose–response relationship between loading frequency and cortical bone (re)modeling reaching a plateau with frequencies beyond 10 Hz has been found.[31] The

mechanism for this nonlinear frequency response is not known, but the authors also confirmed, based on strain gauge measurements, that no dampening of the mechanical loading associated with frequencies beyond 10 Hz occurred. Using the rat tibia four-point bending model, cortical bone responded to frequencies even of 0.5 Hz and above, but not to lower frequencies anymore.[32]

More recently, using the rat ulna axial loading model, it was found that cortical bone formation increased successively with increasing loading frequency up to 10 Hz.[30] Bone healing around a roughened implant was found to be improved by loading the functionally isolated turkey ulna at a frequency of 20 Hz rather than at 1 Hz.[29] These data seem to indicate that an increase in loading frequency results in an increase in the adaptive response of cortical bone. However, the effects of frequency should not be isolated from the effects of the cycle number.[33] At a constant frequency, the proliferate response of human bone-derived grown cells increased with the number of applied cycles until a maximum of 1,800 cycles was reached. Data suggest that the number of applied load cycles within a given time frame plays an important role in bone structural adaptation in vivo as well.[29]

Recent research has shown trabecular bone to be responsive to very low-magnitude mechanical stimuli (0.3 g/5 $\mu\varepsilon.s^{-1}$) introduced at high frequency (30 Hz).[5,34] It is possible that the mechanotransductive pathways in cortical and trabecular bone differ, and that the pathways respond differently to an equivalent mechanical stimulus. Nowadays, several reports suggest that osteocytes, which are terminally differentiated osteoblasts and which are present throughout the entire mineralized bone matrix, are the primary candidates for bone mechanosensing.[35–37] In particular, it is hypothesized that bone interstitial fluid flow through the canalicular network, which is induced by fluid pressure gradients in the deforming bone matrix, activates certain intracellular processes in the osteocytes. Biochemical signals, released by the osteocytes, would then, in turn, regulate osteoblastic and osteoclastic activity.[37]

This study explored a potential animal model showing that the in vivo force can be controlled experimentally to study quantitative biomechanical-mediated bone adaptation under various loading situations. Eventually, this may lead to a better understanding of improved early/immediate loading protocols of, for example, oral implants in humans. Differences in bone modeling rates between the guinea pig and humans limit the extrapolation of the present data in terms of absolute values. Therefore, suggested principles of bone adaptation should be simulated first through individualized finite element modeling and validated to the results of the animal experiment before these can be considered for extrapolation to bone tissue application in humans.

CONCLUSION

The present data show an increase of the BM around controlled early-loaded implants. The effect of early mechanical loading of peri-implant bone is strongly dependent on strain and frequency for a constant period of loading at a constant strain rate. Within these constraints, this cortical bone model has been shown to be most sensitive for high force loading at low frequency.

ACKNOWLEDGMENTS

This research was funded by the European Community: IMLOAD QLK6-CT-2002–02442. Ing. S. Goovaerts and J. Vanhulst are acknowledged for technical support. Sylvia Cerere (Biostatistical Centre, School of Public Health, Leuven, Belgium) is acknowledged for statistical analysis of the data.

REFERENCES

1. Turner C. Three rules for bone adaptation. Bone 1998; 23:399–407.
2. Rubin C, Turner AS, Mallinckrodt C, Jerome C, McLeod K, Bain S. Mechanical strain, induced noninvasively in the high-frequency domain, is anabolic to cancellous bone, but not cortical bone. Bone 2002; 30:445–452.
3. Huja SS, Katona TR, Burr DB, Garetto LP, Roberts WE. Microdamage adjacent to endosseous implants. Bone 1999; 25:217–222.
4. Duyck J, Ronold HJ, Van Oosterwyck H, Naert IE, Vander Sloten J, Ellingsen JE. The influence of static and dynamic loading on the marginal bone behaviour around implants: an animal experimental study. Clin Oral Implants Res 2001; 12:207–218.
5. Heitz-Mayfield LJ, Schmid B, Weige C, et al. Does excessive occlusal load affect osseointegration? An experimental study in the dog. Clin Oral Implants Res 2004; 15:259–268.
6. De Smet E, Jaecques SVN, Jansen JJ, Wevers M, Vander Sloten J, Naert I. The effect of strain amplitude on peri-implant bone (re)modelling: a guinea pig experimental study. Proc Comput Meth Biomech Biomed Eng 2005; 1 (Suppl):61–62.

7. De Smet E, Jaecques SVN, Wevers M, et al. A guinea pig experimental study on the effect of controlled early mechanical implant loading on bone healing and bone mass: an in vivo micro-CT follow-up and histological study. Eur J Oral Sci 2006; 114:232–242.
8. Jaecques SVN, Van Oosterwyck H, Muraru L, et al. Individualized, micro CT-based finite element modelling as a tool for biomechanical analysis related to tissue engineering of bone. Biomaterials 2004; 25:1683–1696.
9. De Smet E, Jaecques SVN, Jansen JJ, Walboomers F, Vander Sloten J, Naert I. Effect of constant strain rate, composed of varying amplitude and frequency, of early loading on peri-implant bone (re)modelling. J Clin Periodontol 2007; 34:618–624.
10. Frost HM. Bone "mass" and the "mechanostat": a proposal. Anat Rec 1987; 219:1–9.
11. Frost HM. A determinant of bone architecture: the minimum effective strain. Clin Orthop 1983; 175:286–292.
12. Rubin C, Lanyon L. Regulation of bone mass by mechanical strain magnitude. Calcif Tissue Int 1985; 37:411–417.
13. Turner CH, Forwood MR, Rho JY, Yoshikawa T. Mechanical loading thresholds for lamellar and woven bone formation. J Bone Miner Res 1994; 9:87–97.
14. Hsieh YF, Robling AG, Ambrosius WT, Burr DB, Turner CH. Mechanical loading of diaphysial bone in vivo: the strain threshold for an osteogenic response varies with location. J Bone Miner Res 2001; 16:2291–2997.
15. Frost HM. Perspectives: bone's mechanical usage windows. Bone Miner 1992; 19:257–271.
16. Bonewald LF, Johnson ML. Osteocytes, mechanosensing and Wnt signaling. Bone 2008; 42:606–615.
17. Kinney JH, Lane NE, Haupt DL. In vivo, three-dimensional microscopy of trabecular bone. J Bone Miner Res 1995; 10:264–270.
18. Jaecques SVN, De Smet E, Jansen JA, et al. The guinea pig as an animal model for the study of immediately loaded implants: a feasibility study. Int J Artif Organs 2001; 24:546.
19. Brouwers JEM, Van Rietbergen B, Huiskes R. No effects of in vivo micro-CT radiation on structural parameters and bone marrow cells in proximal tibia of Wistar rats detected after eight weekly scans. J Orthop Res 2007; 25:1325–1332.
20. Van Der Linden JC, Homminga J, Verhaar JA, Weinans H. Mechanical consequences of bone loss in cancellous bone. J Bone Miner Res 2001; 16:457–465.
21. Van Der Linden JC, Birkenhager-Frenkel DH, Verhaar JA, Weinans H. Trabecular bone's mechanical properties are affected by its non-uniform mineral distribution. J Biomech 2001; 34:1573–1580.
22. Suetens P. Fundamentals of medical imaging. Cambridge: Cambridge University Press, 2002.
23. Stoppie N, Van Der Waerden J-PCM, Jansen JA, Duyck JAJ, Wevers MGT, Naert IE. The validation of microfocus computed tomography for the evaluation of bone-implant specimens. Clin Implant Dent Relat Res 2005; 7:87–94.
24. Robling AG, Duijvelaar KM, Geevers JV, Ohashi N, Turner CH. Modulation of appositional and longitudinal bone growth the rat ulna by applied static and dynamic force. Bone 2001; 29:105–113.
25. Jagger CJ, Chambers TJ, Chow JW. Stimulation of bone formation by dynamic mechanical loading of rat caudal vertebrae is not suppressed by 3-amino-1-hydroxypropylidene-1-bisphosphonate (AHPrBP). Bone 1995; 16:309–313.
26. Mosley JR, Lanyon LE. Strain rate amplitude as a controlling influence on adaptive modelling in response to dynamic loading of the ulna in growing male rats. Bone 1998; 23:313–318.
27. Robling AG, Hinant FM, Burr DB, Turner CH. Improved bone structure and strength after long-term mechanical loading is greatest if loading is separated into short bouts. J Bone Miner Res 2002; 17:1545–1554.
28. Judex S, Gross TS, Zemicke RF. Strain gradients correlate with sites of exercise-induced bone-forming surfaces in the adults skeleton. J Bone Miner Res 1997; 12:1737–1745.
29. Rubin CT, McLeod KJ. Promotion of bony ingrowth by frequency-specific, low-amplitude mechanical strain. Clin Orthop 1984; 298:165–174.
30. Hsieh YF, Turner CH. Effects of loading frequency on mechanically induced bone formation. J Bone Miner Res 2001; 16:918–924.
31. Warden SJ, Turner CH. Mechanotransduction in cortical bone is most efficient at loading frequencies of 5–10 Hz. Bone 2004; 34:261–270.
32. Turner CH, Owan I, Takano Y. Mechanotransduction on bone: role of strain rate amplitude. Am J Physiol 1995; 269:438–442.
33. Kaspar D, Seidl W, Neidlinder-Wilke C, Beck A, Claes L, Ignatius A. Proliferation of human-derived osteoblast-like cells depends on the cycle number and frequency of uniaxial strain. J Biomech 2002; 35:873–880.
34. Rubin C, Turner AS, Bain S, Mallinckrodt C, McLeod K. Low mechanical signals strengthen long bones. Nature 2001; 412:603–604.
35. Weinbaum S, Cowin SC, Zeng Y. A model for the excitation of osteocytes by mechanical loading induced bone fluid shear stresses. J Biomech 1994; 27:339–360.
36. Cowin SC, Weinbaum S, Zeng Y. A case for bone canaliculi as the anatomical site of strain generated potentials. J Biomech 1995; 28:1281–1297.
37. Burger EH, Klein-Nulend J. Responses of bone cells to biomechanical forces in vitro. Adv Dent Res 1999; 13:93–98.